NRC Publications Archive
Archives des publications du CNRC

Moisture transport across interfaces between autoclaved aerated concrete and mortar
Qiu, X.; Haghighat, F.; Kumaran, M. K.

NRC Publications Record / Notice d'Archives des publications de CNRC:
https://nrc-publications.canada.ca/eng/view/object/?id=39100fe7-0a03-4f34-9d68-3ca5668c4dd2
https://publications-cnrc.canada.ca/fra/voir/objet/?id=39100fe7-0a03-4f34-9d68-3ca5668c4dd2

National Research Council Canada   Conseil national de recherches Canada

Canada

NRC·CNRC

**Moisture transport across interfaces between
autoclaved aerated concrete and mortar**

Qiu, X.; Haghighat, F.; Kumaran, M.K.

NRCC-46411

http://irc.nrc-cnrc.gc.ca/ircpubs

MOISTURE TRANSPORT ACROSS INTERFACES BETWEEN AUTOCLAVED AERATED CONCRETE AND MORTAR

Xiaochuan Qiu[1], Fariborz Haghighat[1] and Mavinkal K. Kumaran[2]

ABSTRACT

Experiments were carried out to study the moisture transport across bonded or natural contact interface between AAC and mortar. Bonded contact, in the present study, refers to the contact between two building materials involving penetration of pore structure with a bonding agent, while natural contact refers to the good physical contact between two building material without penetration of pore structure. The moisture content profiles were measured using gamma ray spectrometer. The experimental results showed that, for both types of contact, the assumption of imperfect hydraulic contact is more appropriate than the widely used assumption, perfect hydraulic contact. Furthermore, the latter assumption may result in significant error in predicting moisture transport. The mismatching resistance was assumed in the study to explain the impact of imperfect hydraulic contact on the moisture transport. In addition, a numerical model was developed to calculate the moisture transport in multi-layered materials and was applied to estimate either the mismatching resistance of the interface or the resistance of air films. For a specimen without an interface the agreement between model prediction and experimental results was good. It was found that mismatching resistance of the interface varied with moisture content, the type of source material and the interface with the sink material. This study indicates that the bonded interface can be approximately treated as the natural contact interface, while the presence of an air gap between AAC and AAC could significantly increase the resistance to moisture transport from one material to another.

[1]Dept of Building, Civil and Environmental Engineering, Concordia University, Montreal, Quebec, Canada
[2]Institute for Research in Construction, National Research Council Canada, Ottawa, Ontario, Canada

NOMENCLATURE

D_w moisture diffusivity coefficient (m^2/s)

g gravity acceleration (m/s^2)

h height of the material or assembly (m)

K moisture conductivity coefficient (s)

q flow rate (kg/m^2s)

P_c capillary pressure (Pa)

R_m mismatching resistance of the interface (m/s)

R_v gas constant for water vapor (461.5J/kg·K)

T   temperature (K)

t time (s)

Δz Thickness of the air layer between two adjacent materials (m).

w moisture content (kg/m^3)

w_0 initial moisture content (kg/m^3)

c_{pa} specific heat capacity of air (J/kgK)

v velocity (m/s)

Greek symbols

ρ density (kg/m^3)

β convection mass transfer coefficient for water vapor (kg/m^2sPa)

δ_p water vapor permeability of the material (kg/m·s·Pa)

δ_{pa} water vapor permeability of air (kg/m·s·Pa)

α convection heat transfer coefficient (W/m^2K)

ϕ Relative humidity (--)

Subscripts

1 first layer

2 second layer

a air

l liquid water

v water vapor

cap capillary saturation

INTRODUCTION

Over past two decades, a great deal of concern has been placed on moisture accumulation in building envelopes. This is because that, the moisture accumulation in the building

envelope causes various problems including increased energy use, growth of mold, fungi and bacteria, and increased expense for maintenance of buildings. Because the moisture transport through the building envelope often involves interface phenomena, it is important to gain better understanding of the moisture transport across interfaces between building materials. The study considers both natural contact and bonded contact interfaces in AAC and between AAC and type S mortar (one part of Portland cement, half part of hydrated lime, four parts of sand and one part of water). The bonded interface provides attachment through interactions of the materials. When two specimens have good physical contact without introduction of a filler material at the interface, the contact between such two materials is considered as natural contact interface in the study. Although the mechanisms of moisture transport in a single building material have been extensively studied (e.g., Bear *et al*. 1990, Bedford *et al*. 1983, Greenkorn 1983, and Künzel 1995), the hydraulic characteristics of natural and bonded interfaces are still not well understood and thereby, the simplified assumption of perfect hydraulic contact, is widely used in hygrothermal models (e.g., Wilson *et al*. 1995, Burch *et al*. 1997, Karagiozis *et al*. 2001, and Nofal *et al*. 2001). The assumption of perfect hydraulic contact implies that the interface will have no effect on moisture transport (Pel 1995). In contrast to it, the assumption of imperfect hydraulic contact implies that the interface between building materials will resist the moisture transport. Such an interface is therefore called as imperfect hydraulic contact interface. Measurements have been carried out to investigate whether the assumption of perfect hydraulic contact is appropriate for the real samples.

Pel (1995) studied performance of bonded materials made of clay brick and mortar through the free water intake (imbibition) tests and concluded that the bonded interface between fired-clay brick and mortar added additional resistances for moisture transport. Pel's study revealed that, the assumption of perfect hydraulic contact may not be correct

3

for bonded contact materials composed of brick and mortar. De Freitas *et al.* (1996) investigated the natural contact interfaces between autoclaved aerated concrete and clay brick, and concluded that the natural contact interface between autoclaved aerated concrete and clay brick was imperfect hydraulic contact. Brocken (1998) investigated moisture accumulation in bonded materials made of fired-clay brick and mortar, and concluded that the bonded contact interface between fired-clay brick and mortar had no significant impact on the moisture transport.

Although previous studies resulted in some important findings, the following issues are still unknown:

➢ The source of imperfection of the interface has not been identified.

➢ The characteristics of the imperfect hydraulic contact interface have not been fully established.

➢ The effect of the direction of flow across the interface from one specimen to another on imperfection of the interface has not been established.

➢ The effect of the bond between building materials on moisture transport has not been fully established.

This paper presents the results of a series of experiments designed to study above issues and describes the development of a numerical model used to evaluate the resistance of the interface between AAC and S-mortar as well as the resistance of an air gap between two specimens of AAC.

PART 1: EXPERIMENTAL RESEARCH

Test Materials

Measurements of moisture transport were made for combinations of specimens made of AAC (**A**utoclaved **A**erated **C**oncrete) and S type mortar (S-mortar). All AAC specimens used in the present study were cut from the same block of AAC, which was manufactured

in the USA and aged one year. All S-mortar experiments were made following specifications of ASTM C270-99b and the mixing was carried out under room condition (23°C and 50%RH). The S-mortar specimens were prepared in wood molds. After filling, the molds were covered with damp cloths and kept at room condition for 24 hours. Next the specimens were removed from the molds and were kept at room condition for 28 days before testing. Properties of both materials were experimentally determined and some of them are listed in Table 1.

Table 1. Material properties of AAC and S-mortar

Material	Density (kg/m^3)	Total porosity (%Volume)	Capillary water content (kg/m^3)	Water vapor permanence (kg/m^2sPa)	Water absorption coefficient $(kg/m^2s^{1/2})$
AAC	455 ± 20	75	365	9.27e-10	0.053
S-mortar	1840 ± 60	25.4	187	7.87E-10	0.032

Water vapor permeability of AAC and S-mortar were measured at three conditions, namely 50%, 70% and 90%RH. The resistances of the air layers inside the cup and at surfaces of specimens were taken into account (see Lackey *et al.* 1997). The specimens reached the equilibrium in the temperature and humidity (22.92±0.03°C, 50.6±0.1%RH) before testing. The water vapor permeability results are shown in Figure 1. The sorption isotherms and moisture retention curves of AAC and S-mortar were measured using three relative humidity chambers and three pressure plate chambers with 5, 15 and 100bar, respectively (Jodoin 1997). The results are shown in Table 2. The specimens were dried in a 50°C oven before measuring sorption isotherm and were saturated at capillary water content before measuring moisture retention curve. Moisture diffusivities of AAC and S-mortar were determined using Boltzmann transformation (Marchand *et al.* 1994, and Kumaran 1999) of the data measured by gamma – ray attenuation technique (Kumaran *et al.* 1985, and Kumaran *et al.* 1989). The results are shown in Table 3. Prior to the measurement, the specimens reached the equilibrium in a chamber (22.92±0.03°C,

5

50.6±0.1%RH). The pore size distributions of AAC and S-mortar were measured using image analysis system (Diamond 2000) and shown in Table 4. The porous space of AAC is dominated by pores with diameter over 500μm, while the porous spaces of S-mortar are dominated by pores with diameter between 500μm and 1000μm.
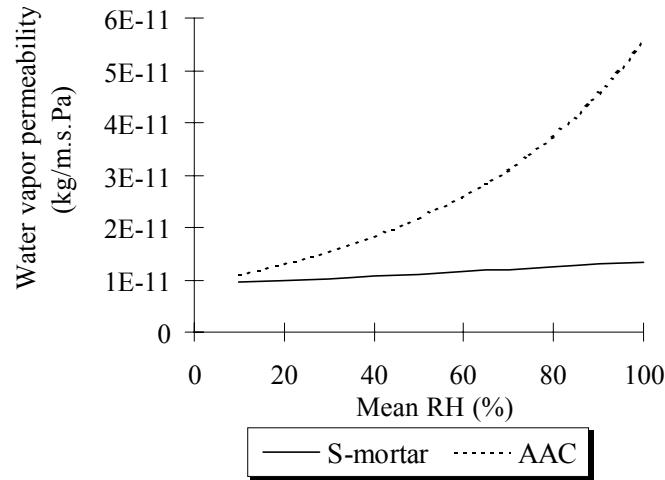

Figure 1. Water vapor permeability of AAC (449 kg/m^3) and S-mortar (1869 kg/m^3).

Table 2. Moisture retention curves of AAC (450 kg/m^3) and S-mortar (1802 kg/m^3).

AAC			S-Mortar		
Relative humidity (%)	Suction Pressure (Pa)	Moisture content (kg/m^3)	Relative humidity (%)	Suction Pressure (Pa)	Moisture content (kg/m^3)
99.93	100000	270.03	99.93	100000	167.5
99.63	500000	261.4	99.63	500000	158.2
99.27	1000000	255.2	99.27	1000000	149.2
98.9	1500000	245.5	98.90	1500000	140.0
97.81	3000000	150.1	96.74	4500000	136.4
88.10	17100000	22.2	88.10	17100000	111.0
71.50	45500000	9.5	71.50	45500000	72.2
50.60	92500000	4.9	50.60	92500000	39.5

Table 3. Moisture diffusivities of AAC (456 kg/m^3) and S-mortar (1860 kg/m^3).

AAC		S-Mortar	
Moisture content (kg/m^3)	Moisture diffusivity (m^2/s)	Moisture content (kg/m^3)	Moisture diffusivity (m^2/s)
263.5	1.20E-07	123.5	8.64E-08
258.0	8.21E-08	113.7	4.50E-08
252.4	4.39E-08	105.7	3.56E-08
242.6	2.56E-08	96.1	2.98E-08
226.4	1.53E-08	85.2	2.62E-08
200.5	9.01E-09	77.4	2.47E-08
147.7	4.38E-09	71.5	2.40E-08
86.2	2.31E-09	65.4	2.35E-08

Table 4. Pore size distributions of AAC (461kg/m^3) and S-mortar (1833 kg/m^3).

Diameter of pores (μm)	< 6	6-25	25-100	100-250	250-500	500-1000	1000-1600	>1600
AAC Percentage of area – (%)	0.017	0.051	0.141	0.687	4.217	17.203	14.629	18.828
S-mortar Percentage of area – (%)	0.084	0.100	0.127	0.299	1.177	2.489	1.137	0.538

Experimental Setup and Tests Conditions

Figure 2 shows the experimental setup utilized to study moisture transport across an interface between building materials.
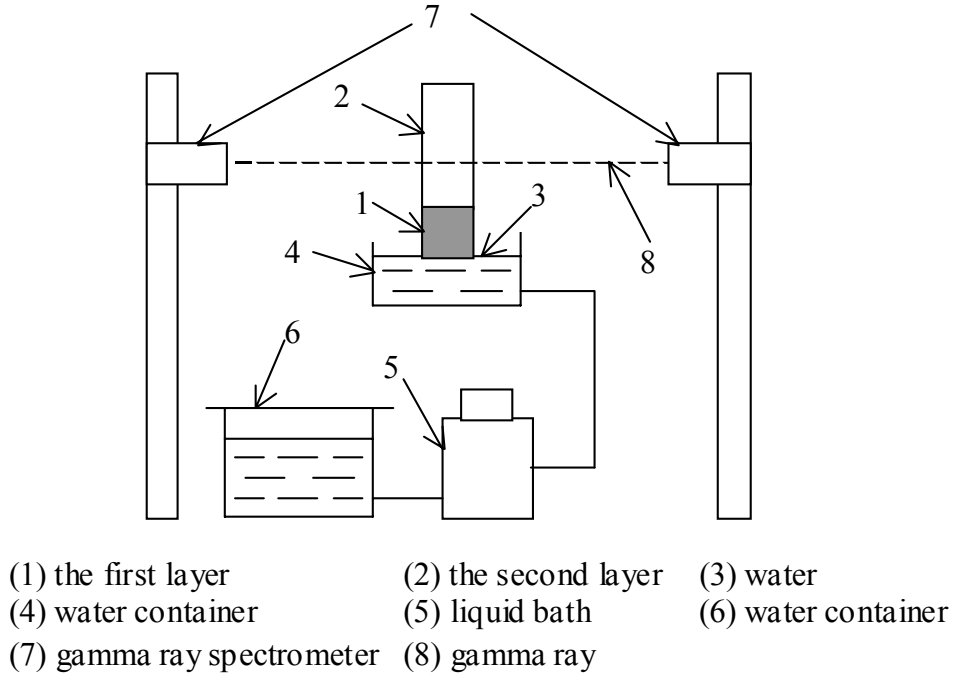
Figure 2. Experimental setup to study moisture transport across the interface

The gamma ray source was Americium ($_{95}Am^{241}$, radioactivity: 7.4×10^9/s). The gamma ray beam emerges from a 2mm ×12mm rectangular hole. The gamma ray spectrometer was interfaced with a computer system that controls and synchronizes the movements of the two platforms carrying the source and detector assemblies. Some parameters such as vertical and horizontal coordinates, and starting time were included into program input data. In the present study, the live time selected for the each measurement was 30s and the experimental determined mass attenuation coefficient of water was 0.0202 m^2/kg (theoretical value: 0.0204 m^2/kg), therefore, the precision was better than 0.2%.

During the tests, the bottom surfaces of the test specimens were in contact with liquid water, which was circulated by a liquid bath and the specimens were scanned by gamma ray spectrometer along their centerlines from bottom to top. The water level in container 4 was kept at constant level up to 3mm – 5mm above the bottom surface of the specimens with help of water container 6. The temperature of water was kept at $22.5 \pm 0.1^{\circ}$C. The

air temperature, relative humidity and velocity were kept at 22 ± 1°C, 49.5 ± 2% and 0.1 ± 0.05m/s, respectively.

Specimens and Tests Procedures

Pieces of AAC were cut from a block using electrical saw. ***Assembly A*** is a single piece of AAC as shown in Figure 3(a). Each surface of another piece AAC was marked and this piece of AAC was cut again into two smaller pieces. To better catch moisture content variation near the interface, the short first layer[3] is preferred due to the time used for gamma ray scanning. In the present study, 30mm is chosen to be thickness of the first layer. These two smaller pieces of AAC were then put together: the two cut surfaces were placed in contact and the vertical surfaces with the same mark were connected. Elastic bands with diameter 100mm that could exert approximately 6 kPa pressure were utilized to ensure a good physical contact. Then, the edge of the interface was sealed with epoxy with approximate thickness of 1mm. Elastic bands were taken off after epoxy dried. This specimen is denoted as the ***Assembly B*** and shown in Figure 3(b).
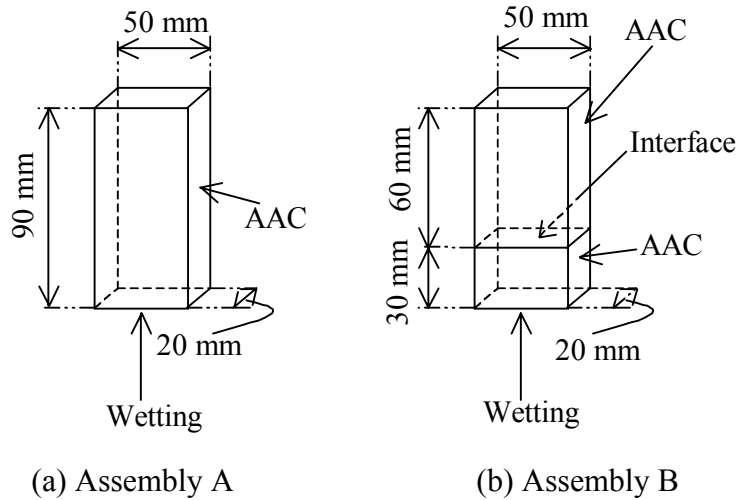

(a) Assembly A   (b) Assembly B

Figure 3. Specimens made from AAC.

---

[3] In the present study, the first layer refers to the material moisture transported from, and the second layer refers to the material moisture transported to.

To prepare bonded or natural contact, pieces of AAC, as shown in Figure 4, were cut from the AAC block. One piece of AAC was bonded with S-mortar at room condition (23°C, 50%RH). The mold used for preparing bonded S-mortar had vertical sides only. After filling, the specimens were covered by damp cloth and the mold was removed after 24 hours. The bonded S-mortar together with AAC was then kept at room condition for 28 days. The open surface of S-mortar was polished using sand paper and the final size of bonded S-mortar is shown in Figure 4 (a). This specimen is denoted as *Assembly C*.

The preparation process of another specimen is similar, except that an acetate fabric with thickness of 0.09mm was placed between AAC and S-mortar to avoid the bonding. It was removed when removing molding, 24 hours after casting. AAC and S-mortar were then placed together to become *Assembly D* in the same manner as it was done for the *Assembly B*. The *Assembly D* was kept at room condition for 28 days and its open surface polished with the sand paper. With identical size, *Assembly C* and *Assembly D* (Figure 4) are suitable to compare the effect of bonding on moisture transport.

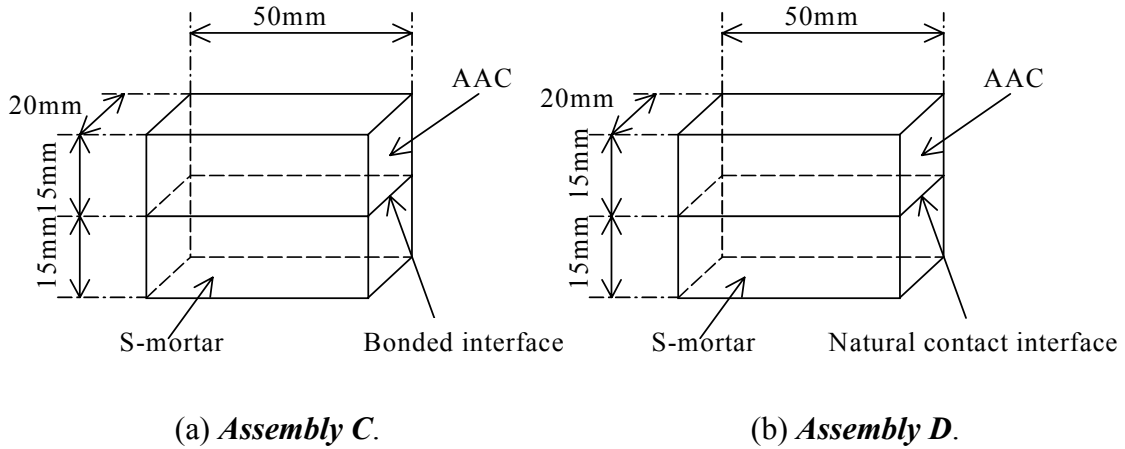

(a) *Assembly C*.   (b) *Assembly D*.

Figure 4. The assemblies made by both S-mortar and AAC.

The vertical sides of all assemblies used in wetting tests were sealed with unfilled epoxy with approximate thickness of 1mm to ensure the 1 − D moisture transport. Prior to

testing, these assemblies were conditioned to equilibrium in a chamber (22.92±0.03°C, 50.6±0.1%RH). For **Assemblies C** and **D**, the free water intake test was performed twice. Firstly with the open surface of S-mortar in contact with water and the open surface of AAC exposed to the ambient air. After the test, the assemblies were dried in a 50°C; conditioned to equilibrium in the same chamber and tested in reverse direction i.e., with the surface of AAC in contact with water and the surface of the S-mortar exposed to the ambient air. To ensure the specimens to reach equilibrium in the temperature humidity chamber (22.92 ± 0.03°C, 50.6 ± 0.1%RH) in relatively short time, thin AAC specimens were preferable yet to measure the distribution of moisture in the specimen, the 15mm thickness was needed. The tests carried out are listed in Table 5.

Table 5. The specimens used in free water intake tests.

Test No.	1	2	3	4	5	6
Assembly	A	B	C		D	
The first layer Thickness (mm) Density (kg/m³)	AAC 90 464	AAC 30 460	AAC 15 454	S-mortar 15	AAC 15 465	S-mortar 15 1845
Contact		Natural	Bonded	Bonded	Natural	Natural
The second layer Thickness (mm) Density (kg/m³)		AAC 60 469	S-mortar 15	AAC 15 454	S-mortar 15 1845	AAC 15 465
Open surface condition	Cut surface	Cut surface	AAC: cut surface / S-mortar: Ground surface		AAC: cut surface / S-mortar: Ground surface	

Experiments Results and Analysis

The moisture content profiles measured with the gamma ray apparatus for **Assemblies A** and **B** during **Tests 1** and **2** are shown in Figures 5 and 6 respectively. The measured moisture content profile of **Assembly C** during **Tests 3** is shown in Figures 7. The measured moisture content profiles of **Assembly C** during **Test 4** and **Assembly D** during

Tests 5 and *6* are shown in the second part of this paper. Because the distances of the interfaces of *Assemblies C* and *D* away wetting surfaces were relatively short, the gamma ray scanned part of each assembly instead of whole assembly to better observe the moisture accumulation near the interface. The moisture content profiles relate the measured values of moisture content (kg/m^3) to the position (mm) relative to the wetting surface and time elapsed since the specimens came into contact with water. The vertical lines on the moisture content profiles represent the positions of the interfaces. The horizontal axis of all figures showing moisture content profile of the specimens indicates the distance away from bottom surface of the specimen, which is set to be zero in those figures.
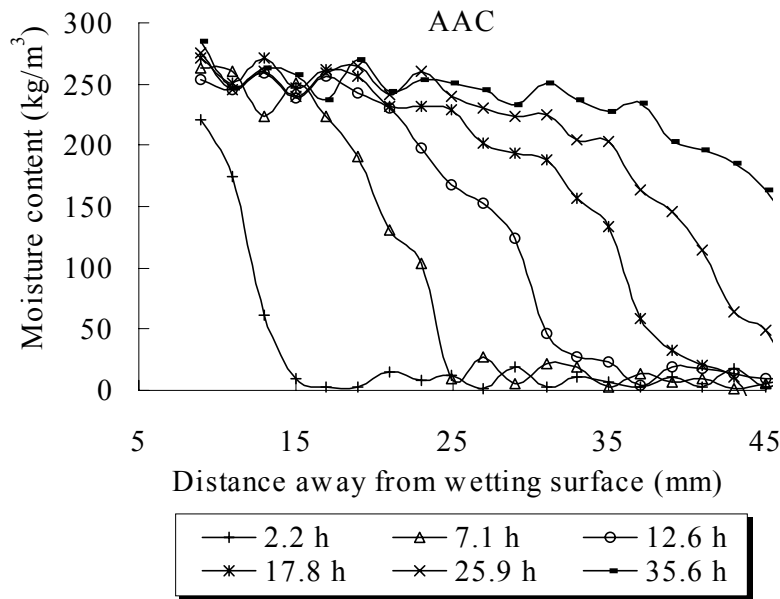

Figure 5. Measured moisture content profile of *Assembly A* (464kg/m^3, 90mm) during *Test 1*, the scale is chosen to better observe the moisture accumulation near the cross section 30mm from the wetted surface of the specimen.
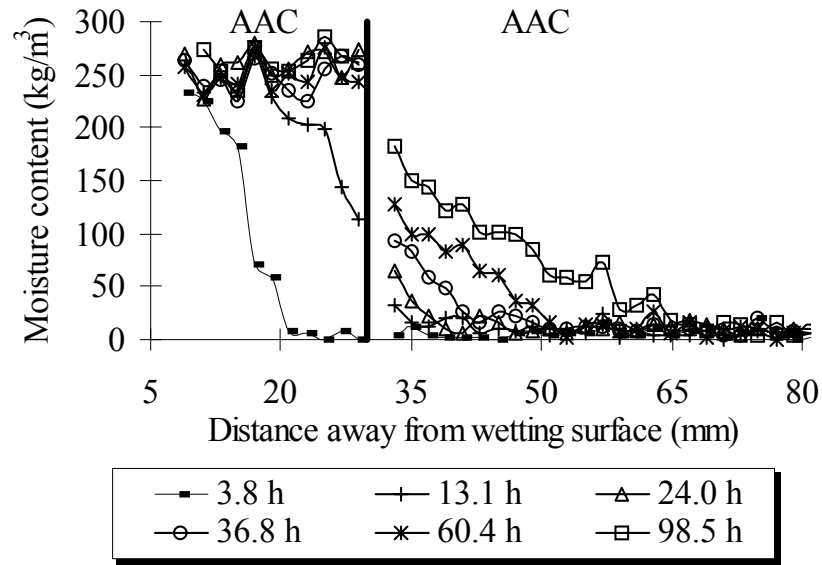
Figure 6. Measured moisture content profile of *Assembly B* (total height: 90mm, the first layer – AAC: 460kg/m^3, 30mm; the second layer – AAC: 469kg/m^3, 60mm; type of contact: natural) during *Test 2*.
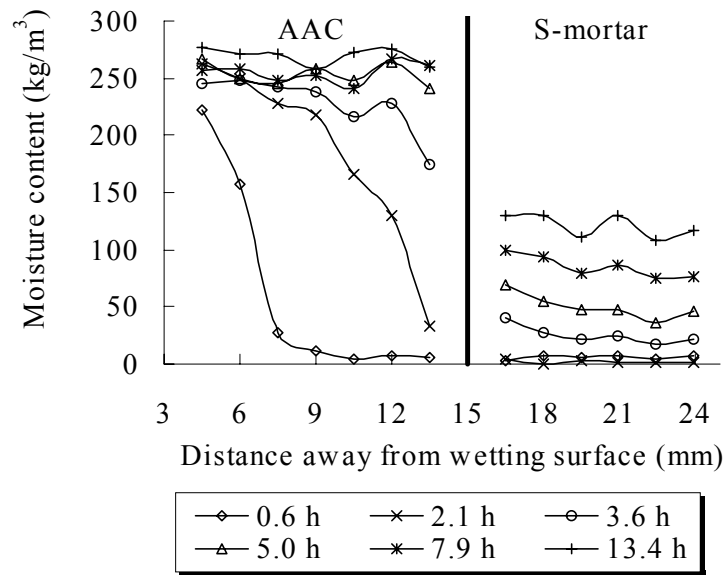

Figure 7. Measured moisture content profile of *Assembly C* during *Test 3* (the first layer – AAC: 454 kg/m^3, 15mm; the second layer – S-mortar: 15mm; type of contact: bonded).

Figure 5 shows that in a single piece of AAC, during wetting process, the distribution moisture content was continuous. Figure 6 shows a drop in moisture content across the natural contact interface between two pieces of AAC. Furthermore, moisture accumulation in the second layer of *Assembly B* was noticeably slower than one shown in Figure 5 (*Assembly A*). Because the same material was used in both layers, the discontinuity of moisture content across the interface indicated that there was a difference in capillary pressure across the interface, i.e., an imperfect hydraulic contact. The slower accumulation of moisture in the second layer suggests that imperfect hydraulic contact interfaces could significantly retard the flow of moisture transport.

For *Assemblies C* and *D*, made of different materials, it is difficult to identify directly whether there was a difference in capillary pressure across the interface between AAC and S-mortar. Yet, the capillary pressure can be derived from moisture retention curves. Using the moisture content at 1.5mm away from the interface shown in Figure 7, the corresponding capillary pressures are shown in Figure 8. Similarly, Figure 9 compares the capillary pressures of S-mortar and AAC at 1.5mm away from the bonded interface for *Test 4* and Figures 10 and 11 show results for *Tests 5* and *6*, respectively.
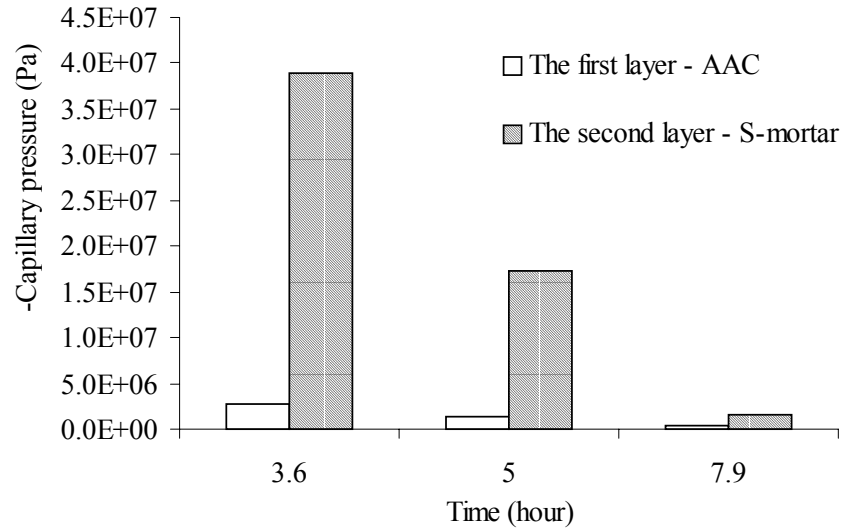
Figure 8. Capillary pressures of AAC and S-mortar at 1.5mm distance from the bonded interface for *Assembly C* during *Test 3* (the first layer – AAC: 454 kg/m^3, 15mm; the second layer – S-mortar: 15mm; type of contact: bonded).
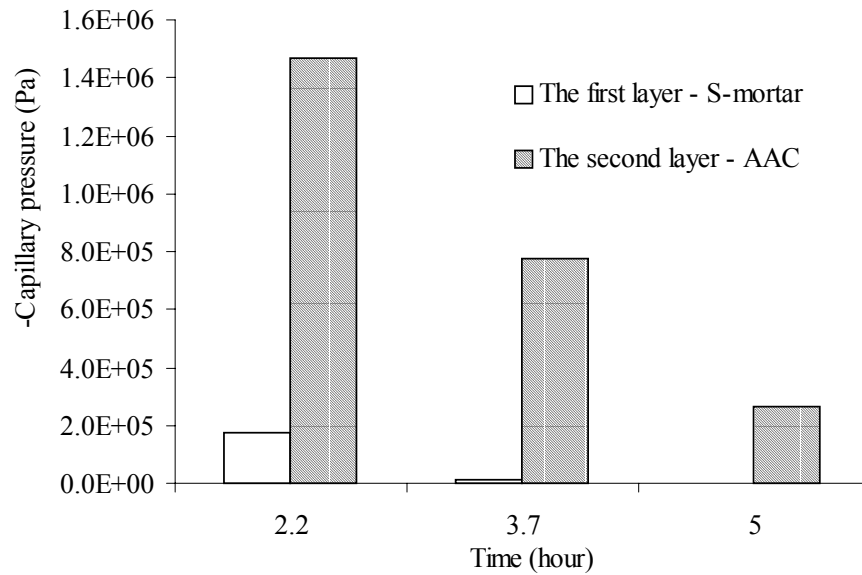

Figure 9. Capillary pressures of AAC and S-mortar at 1.5mm distance from the bonded interface for *Assembly C* during *Test 4* (the first layer – S-mortar: 15mm; the second layer – AAC: 454 kg/m^3, 15mm; type of contact: bonded).

15

Figure 10. Capillary pressures of AAC and S-mortar at 1.5mm distance from the natural contact interface for *Assembly D* during *Test 5* (the first layer – AAC: 465 kg/m^3, 15mm; the second layer – S-mortar: 1845 kg/m^3, 15mm; type of contact: natural).
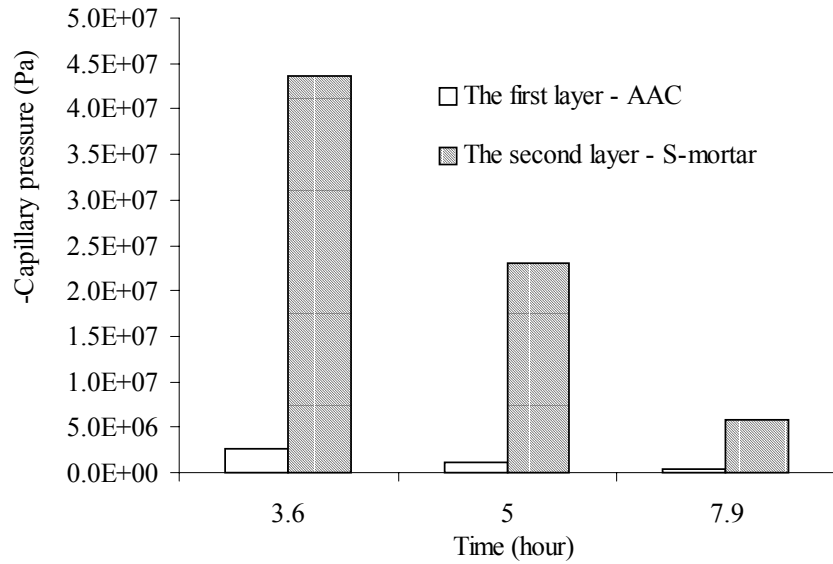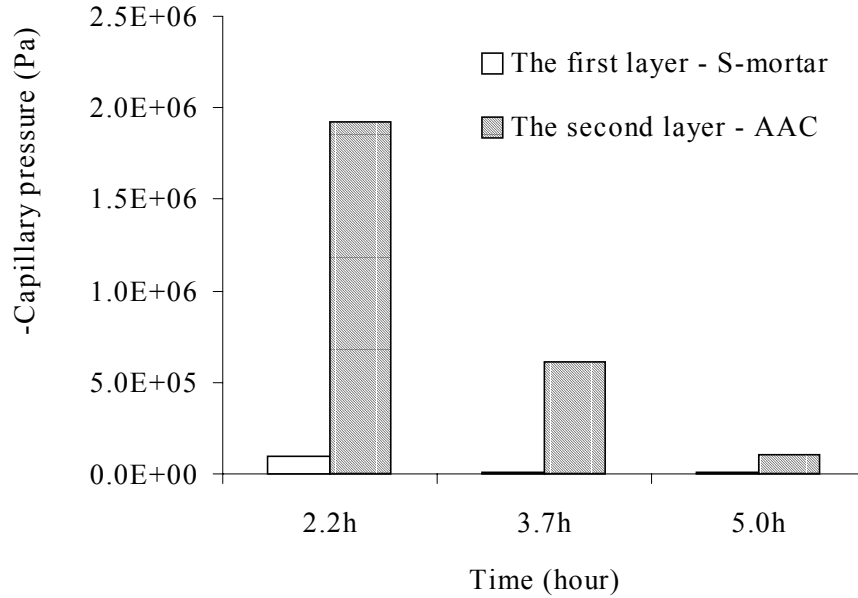

Figure 11. Capillary pressures of AAC and S-mortar at 1.5mm distance from the natural contact interface for *Assembly D* during *Test 6* (the first layer – S-mortar: 1845 kg/m^3, 15mm; the second layer – AAC: 465 kg/m^3, 15mm; type of contact: natural).

Figure 8 shows that, for each measurement, there was a difference in capillary pressure across the bonded interface when moisture is transported from AAC to S-mortar. Similarly, Figures 9 through 11 indicate that, irrespective of the direction of moisture transport, there was a difference in capillary pressure across bonded or natural contact interface between S-mortar and AAC during wetting process. Therefore, neither bonded nor natural contact interface between AAC and S-mortar is perfect hydraulic contact.

Figures 8 through 11 show the similar trend of the presence of varying discontinuity of capillary pressure across imperfect hydraulic contact interface during wetting process. With increasing of moisture content of the two specimens, the discontinuity of capillary pressure across the imperfect hydraulic contact interface between them is more significant at low moisture content than at high moisture content. This may be due to the fact that, the capillary pressure varies with moisture content more significantly at low moisture content than at high moisture content (see Table 2).

The imperfection of an interface may be due to mismatching pore structure of the two specimens. When two materials contact each other, some pores on the contact surfaces are blocked and cannot receive water directly from the first layer as a consequence of mismatching. Therefore, these pores on the contact surface of the second layer have to absorb moisture from other pores. As a consequence, the length of moisture path is increased, even though there is no physical distance between two materials. Therefore, the resistance of the imperfect hydraulic contact is caused by the increased length of the moisture path at interface.

Comparing moisture content profiles of *Assembly C* during *Test 3* and *4* one may see that, moisture accumulation in the second layer is much slower when the moisture transported

from AAC to S-mortar than from S-mortar to AAC. The similar phenomenon is also observed by comparisons of *Tests 5 and 6* (see the second part of the paper). The question is whether this phenomenon is caused by different properties of the second layer alone or also influenced by the properties of the interface. Since it is difficult to obtain detailed information on imperfection of an interface from experimental results only, this question has to be answered with help of modeling. Furthermore, Figures 8– 11 show that performances of bonded and natural contact interfaces are similar. This similarity may imply that the effect of bonding on moisture transport is insignificant i.e., is within the scatter of the experimental results. Therefore, it is imperative combine experimental research with modeling studies to obtain more information from experimental results.

PART 2: MODELING MOISTURE TRANSPORT

Development of a numerical model

The following assumptions were made in the development of a numerical model for predicting moisture transport in the specimens.

(1) Materials are macroscopically homogeneous, isotropic and rigid;

(2) Water vapor is transported by diffusion;

(3) Air is at atmospheric pressure throughout the porous medium;

(4) The liquid water is pure and incompressible;

(5) The hysteresis effect is negligible;

(6) The interface between specimens is imperfect hydraulic contact.

(7) The convection mass transfer coefficient is approximated as a constant

Moisture transport in building material

Since water vapor pressure is significantly lower than the atmospheric pressure, the water vapor can be treated as ideal gas (Lackey *et al.* 1997). Therefore, based on the assumption (2), water vapor transport can be expressed as the well-known equation:

$$q_v = -\delta_p \nabla P_v \tag{1}$$

Liquid water flow in building materials is mainly driven by the gradient of capillary pressure (Künzel 1995). If the gravitational effect was also taken into account, the rate of flow of liquid water in a material can be expressed as:

$$q_l = -K(\nabla P_c + \rho_w \vec{g}) = -D_w\left(\nabla w + \frac{\rho_w \vec{g}}{\partial P_c / \partial w}\right) \tag{2}$$

Based on the mass continuity equation, the following equation can be derived to describe moisture transport in a single porous material:

$$\frac{\partial w}{\partial t} = div\left(D_w \nabla w + \frac{D_w}{\partial P_c / \partial w}\rho_w \vec{g}\right) + div(\delta_P \nabla P_v) \tag{3}$$

Moisture flow across imperfect hydraulic contact interfaces between building materials

Understanding mechanisms of moisture transport in a single material provides a clue for determining liquid water flow across an imperfect hydraulic contact interface. For 1 – D horizontal moisture transport, equation (2) can be rewritten into:

$$q_l = -\frac{dP_c}{dx/K} = -\frac{\Delta P_c}{\frac{1}{K}\cdot \Delta x} = -\frac{\Delta P_c}{R'} \tag{4}$$

Therefore, the liquid water transport is forced by the unbalanced capillary pressure and resisted by 'material resistance', R', which is related to material property, i.e., moisture conductivity, and the distance between positions corresponding to the unbalanced pressures. Similarly, when liquid water transports across an imperfect hydraulic contact interface, the unbalanced capillary pressures at two contact surfaces acts as the potential. The resistance resulting from increased length of moisture path at the interface acts as the 'material resistance', and it is offered by two contact surfaces and is defined as 'mismatching resistance' in the present study. In addition, since the potential of water

vapor transport is water vapor pressure, an interface between two materials with good physical contact is assumed to be perfect for water vapor transport. Therefore, the rate of moisture flow across an imperfect hydraulic contact interface can be expressed as:

$$q = -\left(\frac{P_{c2} - P_{c1}}{R_m} + \delta_{P1} \frac{\partial P_v}{\partial x} \right) \quad (5)$$

When two layers have no real contact, moisture has to be transported from one layer to another in water vapor form. Therefore, the first term of equation (5) is zero and equation (5) becomes:

$$q = -\delta_{pa} \frac{P_{v2} - P_{v1}}{\Delta z} \quad (6)$$

Where δ_{pa} is the water vapor permeability of air (kg/m·s·Pa), Δz is the thickness of the air layer (m), P_{v2} and P_{v1} are the partial vapor pressure of the first layer and second layer at surfaces adjacent the air layer (Pa), respectively.

Initial and boundary conditions during the free wetting process

Some initial conditions and boundary conditions are needed to close moisture transport equations.

(a) *Initial conditions*

For the multi-layered building materials with imperfect hydraulic contact interfaces or with air gap, the initial conditions become:

$$At \ t = 0, \qquad w_i = w_0 \qquad (i=1,2,...n) \quad (7)$$

Where i represents the ith layer relative to the wetting surface.

(b) *Boundary conditions*

For 1 – D free wetting tests, when the bottom surface of the material is in contact with liquid water and the top surface is exposed to the air, boundary conditions of an assembly become:

$$At\ x = 0, \qquad w = w_{cap} \tag{8}$$

$$At\ x = h, \qquad q = \beta \cdot (P_{va} - P_{vl}) \tag{9}$$

Where h is the height of the assembly, P_{vl} is the partial water vapor at the open surface of the last layer, and P_{va} is the partial water vapor pressure of the ambient air.

Numerical solution

A finite control volume numerical method (Patankar 1980) was used to simultaneously solve the above equations and the numerical model MTIMB (*M*oisture *T*ransport *I*n *M*ulti-layered *B*uilding materials) was developed.

Parameter determination:

The material properties such as water vapor permeability, δ_p, and moisture diffusivity coefficient, D_w, and sorption curves can be found either in literatures (e.g., Kumaran 1996) or determined experimentally. Relative humidity, φ, and capillary pressure, P_c, are related by Kelvin's equation:

$$P_c = -\rho_l R_v T \ln \phi \tag{10}$$

Based on the air temperature and relative humidity, the partial water vapor pressure of the air can be determined. The water vapor permeability of air under room temperature was 2×10^{-10} kg·m^{-1}· s^{-1}·Pa^{-1} (Lackey *et al.* 1997). The constant convection mass transfer coefficient, β, can be estimated using Lewis relation (Pedersen 1990):

$$\beta = \frac{\alpha}{R_v T \rho_a c_{pa}} \tag{11}$$

The convection heat transfer coefficient, α, can be estimated from the ambient air velocity by an empirical formula (Pedersen 1990).

$$At\ v_a \le 5\,m/s, \qquad \alpha = 5.82 + 3.96 \cdot v_a \tag{12}$$

Therefore, according to the measured moisture content of the composing materials, the

mismatching resistance can be estimated using model MTIMB.

Model Prediction and Comparison

Firstly, the Test 1 was predicted using model MTIMB and is shown in Figure 12. Since *Assembly A* has no contact, the mismatching resistance is not needed.
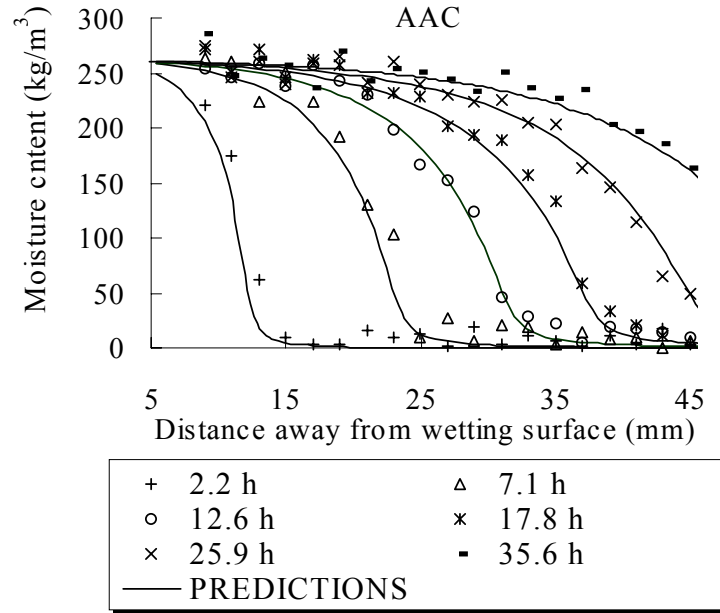

Figure 12. Comparisons of moisture content profiles of *Assembly A* (464 kg/m^3, 90mm) for *Test 1*.

As shown in Figure 12, there is good agreement between predictions of model and experimental results. Therefore, in further application of this model the mismatching resistance can be estimated from a comparison between the model prediction and the experiment involving moisture transport across imperfect hydraulic contact interfaces. If an appropriate mismatching resistance was utilized, sufficient agreement between experimental data and predictions is expected.

Based on curving fitting, the mismatching resistances of *Assemblies C and D* were

estimated. Except for time, all parameters and mismatching resistance are the same for all calculations. Figures 13 and 14 compare the model predictions for *Tests 3* and *4* with experimental results, respectively. Predictions of *Tests 5* and *6* are compared with experimental results in Figures 15 and 16, respectively. The mismatching resistances used in these predictions are shown in Figures 17 and 18. If there is an air layer with a thickness of 5mm between two pieces of AAC in *Assembly B*, moisture content profiles predicted by the model are shown in Figure 19.
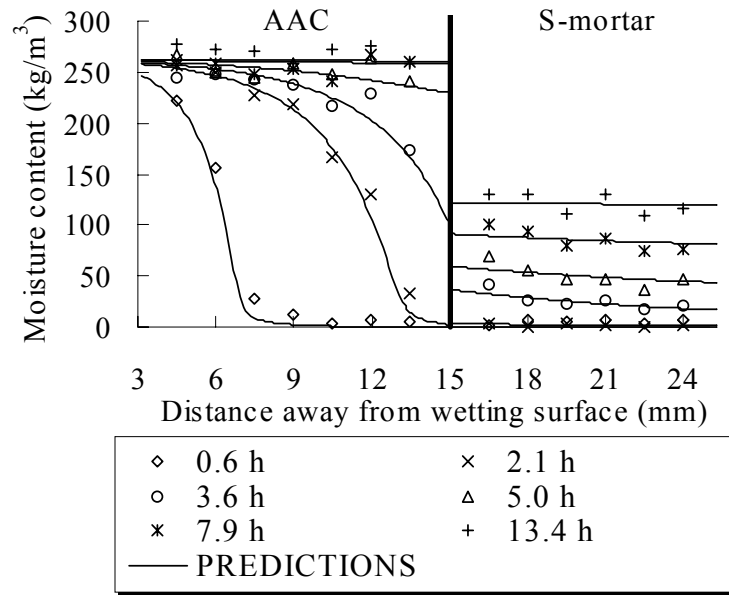

Figure 13 Comparisons of moisture content profiles of *Assembly C* for *Test 3* (the first layer – AAC: 454 kg/m^3, 15mm; the second layer – S-mortar: 15mm; type of contact: bonded).
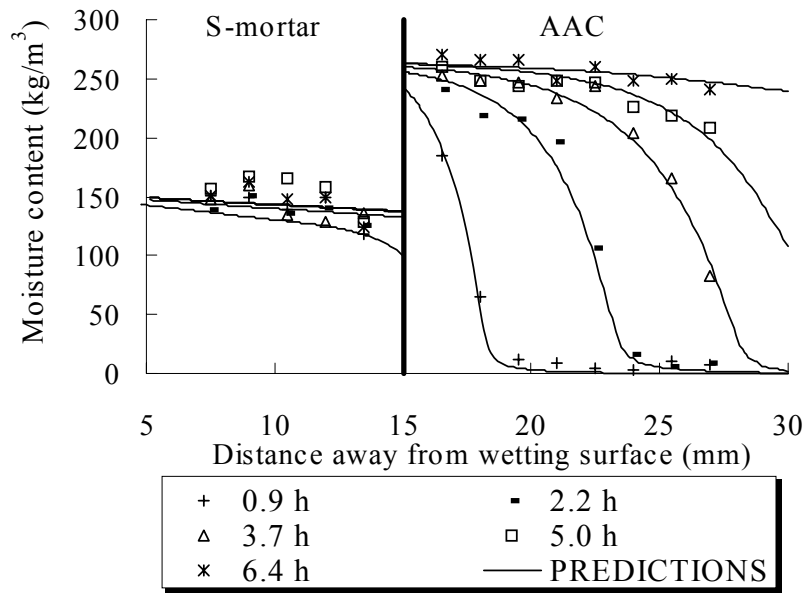
Figure 14 Comparisons of moisture content profiles of *Assembly C* for *Test 4* (the first layer – S-mortar: 15mm; the second layer – AAC: 454 kg/m³, 15mm; type of contact: bonded).
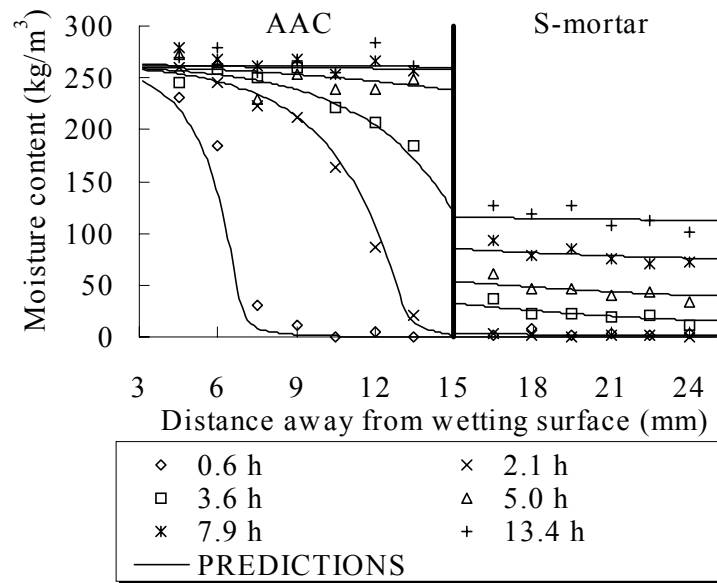

Figure 15 Comparisons of moisture content profiles of *Assembly D* for *Test 5* (the first layer – AAC: 465 kg/m³, 15mm; the second layer – S-mortar: 1845 kg/m³, 15mm; type of contact: natural).
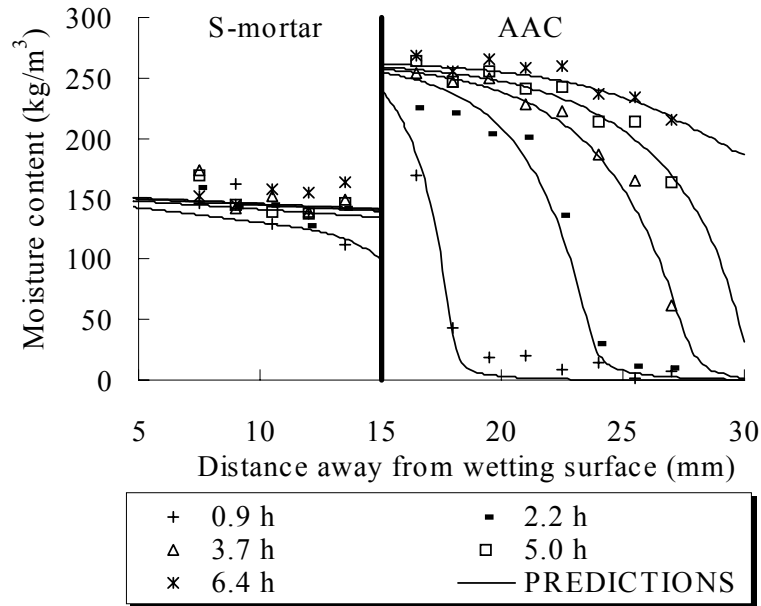
Figure 16. Comparisons of moisture content profiles of *Assembly D* for *Test 6* (the first layer – S-mortar: 1845 kg/m^3, 15mm; the second layer – AAC: 465 kg/m^3, 15mm; type of contact: natural).
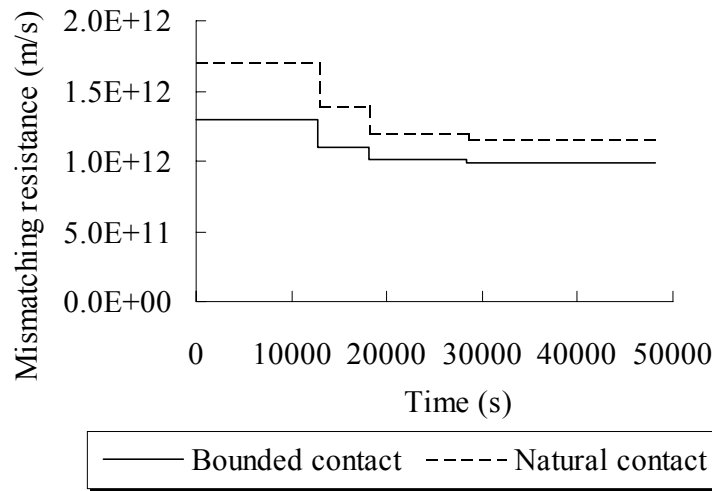

Figure 17. Mismatching resistances of *Assembly C* for *Test 3* (the first layer – AAC: 454 kg/m^3, 15mm; the second layer – S-mortar: 15mm; type of contact: bonded) and *Assembly D* for *Test 5* (the first layer – AAC: 465 kg/m^3, 15mm; the second layer – S-mortar: 1845 kg/m^3, 15mm; type of contact: natural), respectively.
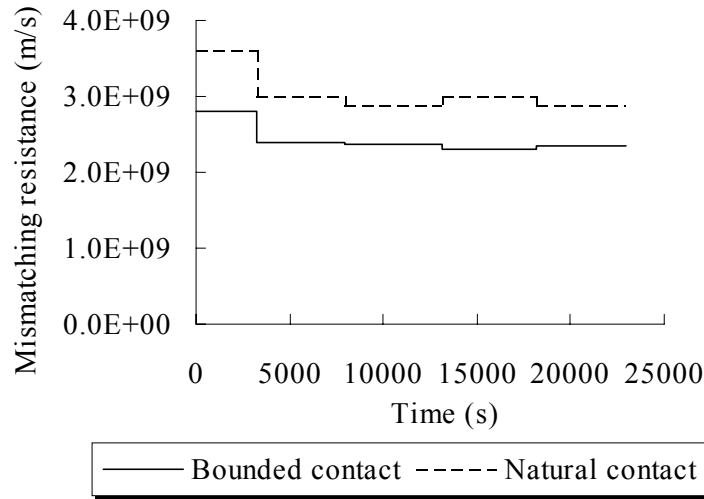
Figure 18. Mismatching resistance of *Assembly C* for *Tests 4* (the first layer – S-mortar: 15mm; the second layer – AAC, 454 kg/m^3, 15mm; type of contact: bonded) and *Assembly D* for *Test 6* (the first layer – S-mortar: 1845 kg/m^3, 15mm; the second layer – AAC: 465 kg/m^3, 15mm; type of contact: natural), respectively.
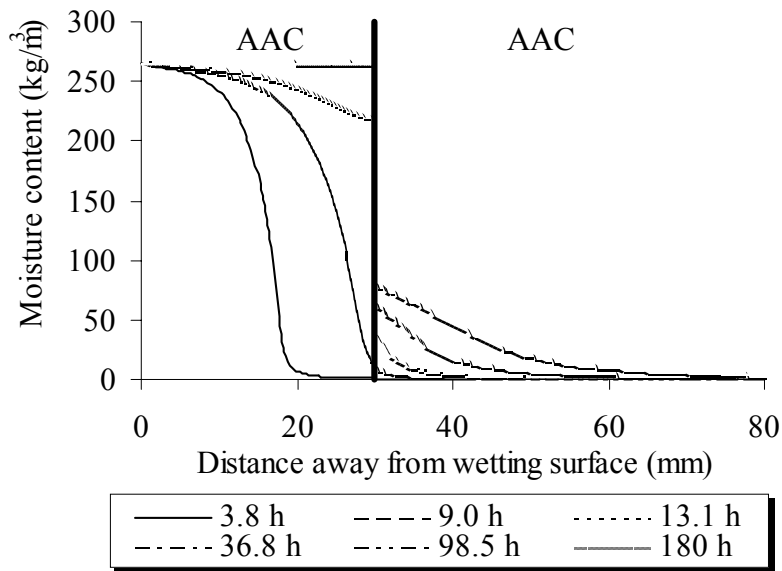

Figure 19. Predicted moisture content profiles of an assembly with 5mm air layer between two pieces of AAC (the first layer – AAC: 30mm; the second layer – AAC: 60mm).

DISCUSSION

Figures 13 and 14 (*assembly C* in *Tests 3 and 4*), show that the predicted moisture profiles agree with experimental results. Similar agreement may be seen in Figures 15 and 16. Therefore, the estimated mismatching resistances (Figures 17 and 18), appear to be correct. Since the conditions of investigated materials used in real buildings may differ from those used in the study, the magnitude of mismatching resistance is more important than actual values determined in this work.

As shown in Figures 17 and 18, for both the bonded and natural contact interface between AAC and S-mortar, mismatching resistance varied during the wetting process. By comparing Figures 13 – 16 with Figures 17 and 18, it is found that the mismatching resistance varies with moisture content of the first layer. At the initial stage of free water intake process, the nature of material porosity, the preferential pore filling function may affect the level of mismatching resistance much more than it would be the case in non-hygroscopic material. Hence, when the first layer reached capillary saturation, the variation of mismatching resistance was smaller after the first layer almost reached capillary saturation than before (see Figures 13 – 18).

Also as shown in Figures 17 and 18, the mismatching resistance (of the bonded or natural contact interface) between AAC and S-mortar was different for the different directions of the moisture transport. For the bonded or natural contact interface between AAC and S-mortar, the mismatching resistance is three orders magnitude larger when moisture transports from AAC to S-mortar than from S-mortar to AAC. Therefore, for the imperfect hydraulic interface resulting from contact of different types of materials, the direction of flow across the interface from one material to another may have significant impact on the mismatching resistance of the interface. The different material properties of AAC and S-mortar may contribute to different mismatching resistances in two cases. In

contrast to S-mortar, AAC has a much higher porosity and contains larger pores. As a consequence, moisture is more easily distributed from those pores connected with the first layer to other blocked pores resulting from mismatching for AAC than S-mortar. Consequently, the increased length of the moisture path at the interface is much shorter in case of moisture transport from S-mortar to AAC than from AAC to S-mortar. Therefore, mismatching resistances in two cases can be different.

Furthermore, as shown in Figures 17 and 18, the mismatching resistance of *Assembly C* was in the same magnitude and varied in the same way as *Assembly D*. This indicates that the bonding between AAC and S-mortar may have no significant impact on the moisture transport and the bonded interface could be approximately treated as the natural contact interface.

Compared to experiment measurements shown in Figure 6, the model predictions shown in Figure 20 indicate that a 5-mm thick layers of air layer could result in much slower moisture accumulation in the second layer than the natural contact interface between two pieces of AAC. This suggests that an air gap between AAC and AAC could significantly resist moisture migration from one material to another.

CONCLUSIONS:

The experimental results showed that a significant resistance could be created by the imperfect hydraulic contact and thereby, the assumption of perfect hydraulic contact may result in significant error in predicting the moisture transport in building material.

A mismatching resistance of the interface was introduced to estimate the effect of imperfect contact. A numerical model was developed to calculate the moisture transport in multi-layered assemblies and applied to estimate the mismatching resistance of the

interface or resistance offered by air films. Through comparing predictions of the model with experimental results, the mismatching resistance was inferred.

First, model predictions were verified against the experimental results obtained on a single specimen. Then, based on curve fitting, the mismatching resistances of bonded and natural contact interfaces between AAC and S-mortar were estimated. It was found that the mismatching resistance decreases as moisture content of the first layer increases, and that it decreases when the first layer reached capillary moisture content. Furthermore, the mismatching resistance of the interface was found to depend on the type of source material and the nature of the surface of the sink material. The difference in mismatching resistance resulting from the direction of moisture flow across the interface varied with three orders of magnitude for the interface between AAC and S-mortar.

It also found that mismatching resistances of both types of interfaces studied were similar, indicating that the bonding between AAC and S-mortar may have insignificant impact on moisture transport, and the bonded interface can be treated as the natural contact interface.

Finally, the model indicated that an air gap introduced within AAC material could significantly increase the resistance of the interface to moisture transport.

ACKNOWLEDGEMENTS

REFERENCES

Bear, J. and Bachmat, Y. (1990), "Introduction to modeling of transport phenomena in porous media," *Kluwer Academic Publishers*, Dordrecht, Netherlands.

Bedford, A. and Drumheller, D.S. (1983), "Theories of immiscible and structured mixtures,"*International Journal of Engineering Science*, Vol. 21, pp. 863-960.

Brocken, H.J.P. (1998), "Moisture transport in brick masonry the grey area between bricks," *Ph.D. Thesis*. Technical University Eindhoven, Netherlands.

Burch, M. and Chi, J. (1997), "MOIST 3.0, A PC program for predicting heat and moisture transfer in building envelopes," *NIST Special Publication* 917.

Greenkorn, R.A. (1983), "Flow phenomena in porous media," *Marcel Dekker, Inc*. New York.

De Freitas, V. P. Abrantes, V. and Crausse, P. (1996), "Moisture migration in building walls – analysis of the interface phenomena," *Building and Environment* Vol. 31(2), pp. 99-108.

Jodoin, A. (1997), "Pressure plate extractor validation," *Internal Report*, National Research Council, Canada.

Diamond, S. (2000), "Mercury porosity, an inappropriate method for the measurement of pore size distributions in cement-based materials," *Cement and Concrete Research* Vol. 30, pp. 1517-1525

Karagiozis A. Künzel, H. and Holm, A. (2001), "WUFI ORNL/IBP Hygrothermal Model," *Proceeding of the 8th conference on building science and technology*, *Solutions to Moisture Problems in Building Enclosures*, pp. 158-183. Toronto, Ontario.

Kumaran, M.K. and Bomberg, M. (1985), "A gamma spectrometer for determination of density distribution and moisture distribution in building materials," *Proceedings of the international symposium on moisture and humidity*, pp. 485-490.Washington, D.C.,

Kumaran, M.K. and Mitalas, G.P. Kohonen, R. and Ojanen, T. (1989), "Moisture transport coefficient of pine from gamma ray absorption measurement," *ASME* Vol. 123,

pp. 179-183.

Kumaran, M.K. (1996),. "IEA ANNEX24: Heat, air and moisture transport, Final report **3**, task 3: material properties," *Laboratorium Bouwfysica*, K.U.-Leuven, Belgium.

Kumaran, M. K. (1999), "Moisture diffusivity of building materials from water absorption measurements," *Journal of Thermal Envelop & Building Science,* Vol. 22, pp. 349-355.

Künzel, H.M. (1995), "Simultaneous heat and moisture transport in building components," *Ph.D. Thesis*, University of Stuttgart, Germany.

Lackey, J. C. Marchand, R. G. and Kumaran, M. K. (1997), "A logical extension of the ASTM standard E96 to determine the dependence of water vapor transmission on relative humidity," *Insulation Materials: Testing and Applications*, Vol. **3**, pp. 456-469.

Marchand, R.G. and Kumaran, M.K. (1994), "Moisture diffusivity of cellulose insulation," *Journal of Thermal Insulation and Building Envelopes*, Vol. **17**, pp. 362-377.

Nofal, M. Straver, M. and Kumaran, K. (2001), "Comparison of four hygrothermal models in terms of long term performance assessment of wood-frame constructions," *Proceeding of the 8th conference on building science and technology, Solutions to Moisture Problems in Building Enclosures*, pp. 119-138. Toronto, Ontario.

Patankar, S. V. (1980), "Numerical heat transfer and fluid flow," *Hemisphere Publishing Corp.* Washington D.C.

Pedersen, C. R. (1990), "Combined heat and moisture transfer in building materials," *Report No. 214*, *Thermal insulation laboratory*. Technical University of Denmark, Denmark.

Pel, L. (1995), "Moisture transport in porous building materials," *Ph.D. Thesis*, Technical University Eindhoven, Netherlands.

Wilson, M. A. and Hoff, W.D. (1995), "Water movement in porous building materials – XIII Absorption into a two – layer composite," *Building and Environment,* Vol.30(2), pp. 209-219.